Journal of Alloys and Compounds 514 (2012) 71–75

Contents lists available at SciVerse ScienceDirect

Journal of Alloys and Compounds

journal homepage: www.elsevier.com/locate/jallcom

Structures of the strontium and barium dodecahydro-*closo*-dodecaborates

Jae-Hyuk Her[a,b,1], Hui Wu[a,b], Nina Verdal[a,*], Wei Zhou[a,b], Vitalie Stavila[c], Terrence J. Udovic[a]

[a] NIST Center for Neutron Research, National Institute of Standards and Technology, 100 Bureau Dr., MS 6102, Gaithersburg, MD 20899-6102, United States
[b] Department of Materials Science and Engineering, University of Maryland, College Park, MD 20742-2115, United States
[c] Sandia National Laboratories, 7011 East Avenue, Livermore, CA 94551-0969, United States

ARTICLE INFO

Article history:
Received 13 September 2011
Received in revised form 23 October 2011
Accepted 24 October 2011
Available online 10 November 2011

Keywords:
$B_{12}H_{12}^{2-}$
Density functional theory
Dodecahydro-*closo*-dodecaborate
Neutron powder diffraction
Phonon density of states
X-ray powder diffraction

ABSTRACT

The structures of the anhydrous alkaline-earth-metal dodecahydro-*closo*-dodecaborates, $SrB_{12}H_{12}$ and $BaB_{12}H_{12}$, were determined by X-ray and neutron powder diffraction methods corroborated by a combination of neutron vibrational spectroscopic data and density-functional-theory-based phonon calculations. Both compounds possess the same novel trigonal structure with *P*31*c* space group symmetry, which appears to represent the most stable arrangement of alkaline-earth cations and dodecahydro-*closo*-dodecaborate anions for cations above a certain size.

Published by Elsevier B.V.

1. Introduction

The structures of the alkali-metal (A) and alkaline-earth-metal (Ae) dodecahydro-*closo*-dodecaborates, $A_2B_{12}H_{12}$ and $AeB_{12}H_{12}$, have recently garnered the interest of researchers in the field of hydrogen storage, since one promising class of materials, the alkali-metal and alkaline-earth-metal borohydrides, ABH_4 and $Ae(BH_4)_2$, is known to decompose under certain dehydrogenation conditions to form $A_2B_{12}H_{12}$ and $AeB_{12}H_{12}$ intermediate species [1]. These species are fairly robust and can be somewhat resistant to rehydrogenation back to the parent borohydride during hydrogen recharging, limiting the hydrogen cycling reversibility of the parent materials. The structures of the lighter alkali-metal (Li and Na) and alkaline-earth-metal (Mg and Ca) dodecahydro-*closo*-dodecaborates have been of particular interest because their corresponding borohydride relatives possess the more favorable hydrogen mass fractions for storage. Indeed, the structures of $Li_2B_{12}H_{12}$ (*Pa*-3 symmetry) [2], $Na_2B_{12}H_{12}$ ($P2_1/n$ symmetry) [3], and $CaB_{12}H_{12}$ (*C*2/*c* symmetry) [4] have been recently reported in the literature. Although there is a theoretically predicted $MgB_{12}H_{12}$ structure with *C*2/*m* symmetry [5], the actual structure still eludes researchers due to the difficulty of synthesizing an undecomposed anhydrous sample [6]. Besides $MgB_{12}H_{12}$, no structure has been reported yet for the heaviest alkaline-earth compounds, $SrB_{12}H_{12}$ and $BaB_{12}H_{12}$. Although not as pertinent to hydrogen-storage research, knowledge of their structures would help to further clarify the unknown relationship between cation size and structural symmetry for the entire series of $AeB_{12}H_{12}$ compounds, similar to what was achieved for the $A_2B_{12}H_{12}$ compounds [3]. We report here the successful structural determinations of both $SrB_{12}H_{12}$ and $BaB_{12}H_{12}$ via a combination of X-ray powder diffraction (XRPD), neutron powder diffraction (NPD), neutron vibrational spectroscopy (NVS), and density functional theory (DFT) calculations.

2. Materials and methods

A $SrB_{12}H_{12}$ sample was synthesized by reacting an aqueous solution of $(H_3O)_2B_{12}H_{12}$ with $SrCO_3$. A ^{11}B-enriched $BaB_{12}H_{12}$ sample was synthesized by ion-exchange of Ba^{2+} cations for the Cs^+ cations in a $Cs_2(^{11}B)_{12}H_{12}$ (>99.8% ^{11}B) starting material obtained from Katchem [7]. (The lack of highly neutron-absorbing ^{10}B in the latter sample allowed for the practical collection of both XRPD and NPD patterns.) The final anhydrous $SrB_{12}H_{12}$ and $BaB_{12}H_{12}$ polycrystalline powders were prepared by the evaporation of solvation waters above 473 K *in vacuo* according to previously published procedures [8].

Since the $SrB_{12}H_{12}$ and $BaB_{12}H_{12}$ compounds were highly hygroscopic, they were loaded into sealed thin-wall glass capillaries. Subsequently, room-temperature (295 K) XRPD patterns were collected in transmission mode using a Rigaku Ultima III sealed-tube (1.6 kW, Cu Kα) diffractometer. The TOPAS-Academic program was used to index the XRPD patterns and to solve and refine the structures.

Neutron scattering measurements were taken at the National Institute of Standards and Technology Center for Neutron Research. An NPD measurement of $BaB_{12}H_{12}$ was performed at 10 K with the BT-1 High-Resolution Powder

* Corresponding author.
E-mail address: nina.verdal@nist.gov (N. Verdal).
[1] Current address: GE Global Research, 1 Research Circle, Niskayuna, NY 12309, United States.

0925-8388/$ – see front matter. Published by Elsevier B.V.
doi:10.1016/j.jallcom.2011.10.085

Diffractometer [9] with the Cu(3 1 1) monochromator at $\lambda = 1.5401(2)$ Å and an in-pile collimation of 15 min of arc. The sample was contained in an Al foil pouch and placed inside a sealed tubular V can. A closed-cycle He refrigerator was used to attain 10 K. Data were collected over the 2θ range of 3–168° with a step size of 0.05°. Wavelength errors were not included in the standard deviations of the structural parameters; *i.e.*, the precisions reported in this paper for the structural parameters reflect the quality of the data and the corresponding refinement model, assuming a fixed neutron wavelength. Profile refinement of the NPD pattern was made by Rietveld analysis using the GSAS code as implemented in EXPGUI [10,11].

The NVS measurements of $SrB_{12}H_{12}$ and $BaB_{12}H_{12}$ were performed at 4 K with the Filter Analyzer Neutron Spectrometer [12] with 20′ horizontal collimations before and after the Cu(2 2 0) monochromator. First-principles calculations were performed within the plane-wave implementation of the generalized gradient approximation to DFT using a Vanderbilt-type ultrasoft potential with Perdew–Burke–Ernzerhof exchange correlation [13]. For comparison with the NVS measurements, the phonon densities of states (DOS) were calculated from the DFT-optimized structure using the supercell method ($2 \times 2 \times 1$ cell size) with finite displacements [14,15] and was appropriately weighted to take into account the H, B, Sr, and Ba total neutron scattering cross sections.

Enthalpic signatures of potential phase transformations for both $SrB_{12}H_{12}$ and $BaB_{12}H_{12}$ at higher temperatures were sought using combined thermogravimetric analysis—differential scanning calorimetry with a Netzsch (STA 449 *F1 Jupiter*) TGA-DSC under He flow between 295 and 950 K.

3. Results and discussion

The $SrB_{12}H_{12}$ and $Ba(^{11}B)_{12}H_{12}$ were found by room-temperature XRPD measurements to be isostructural with trigonal symmetry. The ultimate structure solution for both compounds was first determined from the $SrB_{12}H_{12}$ XRPD data (see Fig. 1) by the direct space searching (simulated annealing) method in space group *P*31*c*. For the initial structure model, an ideal-icosahedron rigid body was defined for the $B_{12}H_{12}^{2-}$ anion, and dynamic occupancy correction was enabled during the annealing process. After decent agreement was achieved between observed and calculated patterns, the structure model was trimmed out by removing duplicated atoms in the rigid-body definition due to the incorporation of molecular and crystallographic symmetry operations. The Rietveld refinement was still performed using a rigid-body model since the XRPD pattern did not contain sufficient information to localize the individual atomic positions, especially due to the insensitivity of X-rays for H atoms. Though the B and H atoms were constrained, the B–B and B–H distances were allowed to vary. All displacement parameters were treated isotropically, and all like atoms were constrained to the same values.

Fig. 2 shows the representative crystal structure of $SrB_{12}H_{12}$ and $BaB_{12}H_{12}$ viewed along the *c*-axis, and Table 1(a) and (b) display

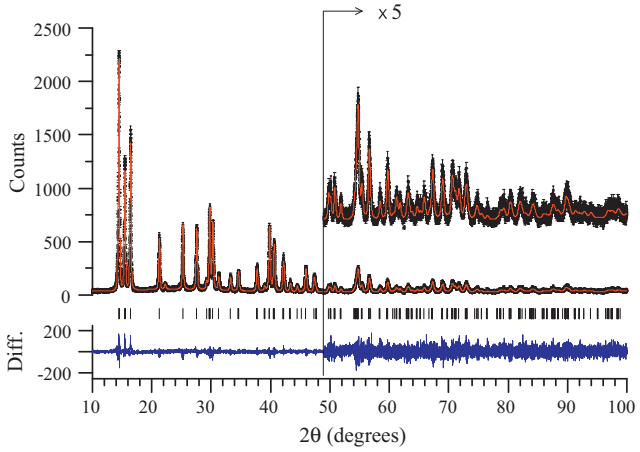

Fig. 1. Observed XRPD pattern (black points) of $SrB_{12}H_{12}$ with the overlay of the Rietveld refinement result (red solid line). The bottom curve (blue) is the difference plot (observed–calculated) on the same vertical scale. Standard uncertainties are commensurate with the scatter in the data. (For interpretation of the references to color in this figure legend, the reader is referred to the web version of the article.)

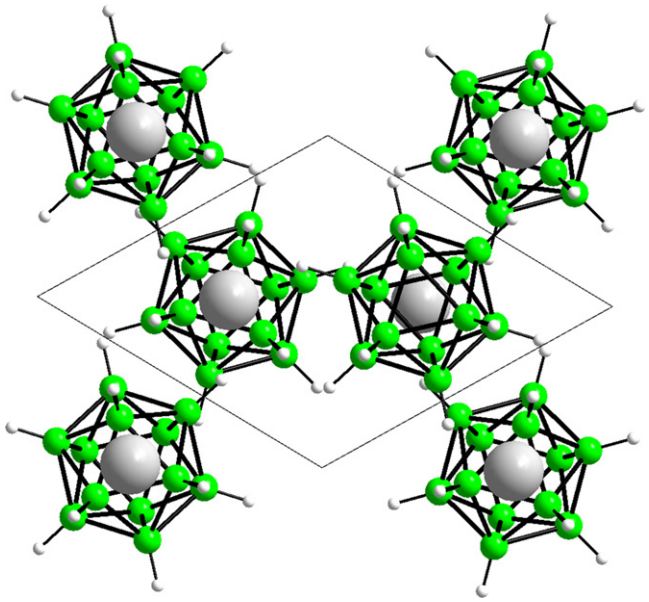

Fig. 2. The structure of $SrB_{12}H_{12}$ and $BaB_{12}H_{12}$ viewed along the *c*-axis: cations (large gray spheres), B (medium green spheres), and H (small white spheres). Thin black lines denote the unit-cell boundary. (For interpretation of the references to color in this figure legend, the reader is referred to the web version of the article.)

the refined structural parameters at 295 K as determined from the XRPD data. Tables S1 and S2 in the Supplemental Information (SI) summarize the corresponding near-neighbor B–B and B–H interatomic distances. The quality of the XRPD data for $BaB_{12}H_{12}$ (see SI Fig. S1) did not justify any relaxations of the rigid-body constraints to allow for distortion of the $B_{12}H_{12}^{2-}$ icosahedron, yielding only single near-neighbor B–B and B–H bond distances of 1.87(2) and 0.9(2) Å, respectively. (Of course, the NPD data should yield more reliable values for distances involving H atoms.) The XRPD data at 295 K indicate a smaller unit cell volume (by ≈9%) for $SrB_{12}H_{12}$ than for $BaB_{12}H_{12}$, a trend expected from their relative radii (*e.g.*, Pauling radii are 1.13 and 1.35 Å for Sr^{2+} and Ba^{2+} cations, respectively [16]). In the *P*31*c* structure, each cation is coordinated tetrahedrally by four $B_{12}H_{12}^{2-}$ anions, and each $B_{12}H_{12}^{2-}$ anion is surrounded tetrahedrally by four cations (see Fig. 3) with distances from the center of the anions to the cations of 4.27 and 4.32 Å for $SrB_{12}H_{12}$ and 4.40 and 4.54 Å for $BaB_{12}H_{12}$ at 295 K. Each $B_{12}H_{12}^{2-}$ anion has three H atoms facing towards the neighboring cation, so each cation is surrounded by a total of twelve H neighbors, as depicted by the dashed blue lines in Fig. 3. The packing diagram is given in Fig. 4, revealing the mutual tetrahedral arrangements of cations and anions in the structure.

The 10 K NPD data for $BaB_{12}H_{12}$ (see Fig. 5) led to the more precise location of the H atoms, and the *P*31*c* structure model was refined without the use of $B_{12}H_{12}^{2-}$ rigid-body constraints. It should be noted that the large incoherent scattering background from H in the NPD data could have been avoided by replacing the H atoms with D atoms, leading to an improved diffraction pattern, but synthesizing or obtaining such a deuterated sample was determined to be impractical at the time. Table 1(c) displays the corresponding structural parameters, and Table S3 in the SI summarizes the resulting B–B and B–H bond distances.

It is evident that the ionic interactions and *P*31*c* packing arrangement lead to measurable distortions of the $B_{12}H_{12}^{2-}$ anion from its ideal icosahedral geometry. Indeed, the NPD results indicate at least three different B–H bond distances (within statistical uncertainty) ranging from 1.129(1) to 1.155(1) Å. In addition, there are ten different B–B covalent bond distances (also within statistical uncertainty), ranging from 1.7385(1) to 1.8997(1) Å. The variation

Table 1
Refined structural parameters for $SrB_{12}H_{12}$ and $Ba(^{11}B)_{12}H_{12}$ (*P*31*c*, No. 159).

Atom	Site	Frac.	*x*	*y*	*z*	U_{iso}
(a) $SrB_{12}H_{12}$: XRD at 295 K; a = 7.0529(2) Å, c = 11.4414(4) Å; R_{wp} = 0.1204, R_p = 0.0896, and χ^2 = 1.088						
Sr	2*b*	1.0	2/3	1/3	1/4	0.94(5)
B1	6*c*	1.0	0.9235(1)	0.3979(1)	0.9055(1)	0.0(2)
B2	6*c*	1.0	0.5069(1)	0.2966(1)	0.9918(1)	0.0(2)
B3	6*c*	1.0	0.8264(1)	0.3701(1)	0.7622(1)	0.0(2)
B4	6*c*	1.0	0.4098(1)	0.2688(1)	0.8485(1)	0.0(2)
H1	6*c*	1.0	0.0851(1)	0.4385(1)	0.9235(1)	0.0(2)
H2	6*c*	1.0	0.4064(1)	0.2735(1)	0.0641(1)	0.0(2)
H3	6*c*	1.0	0.9269(1)	0.3932(1)	0.6900(1)	0.0(2)
H4	6*c*	1.0	0.2483(1)	0.2282(1)	0.8305(1)	0.0(2)
(b) $Ba(^{11}B)_{12}H_{12}$: XRD at 295 K; a = 7.293(1) Å, c = 11.762(2) Å; R_{wp} = 0.0713, R_p = 0.0568, and χ^2 = 1.141						
Ba	2*b*	1.0	2/3	1/3	1/4	0.0(2)
B1	6*c*	1.0	0.93(3)	0.38(3)	0.89(1)	0(2)
B2	6*c*	1.0	0.51(1)	0.30(2)	0.98(1)	0(2)
B3	6*c*	1.0	0.83(1)	0.36(2)	0.74(3)	0(2)
B4	6*c*	1.0	0.41(3)	0.28(3)	0.84(2)	0(2)
H1	6*c*	1.0	0.1(2)	0.4(2)	0.91(8)	0(2)
H2	6*c*	1.0	0.4(1)	0.3(1)	0.04(9)	0(2)
H3	6*c*	1.0	0.9(1)	0.4(1)	0.68(9)	0(2)
H4	6*c*	1.0	0.28(8)	0.3(1)	0.82(6)	0(2)
(c) $Ba(^{11}B)_{12}H_{12}$: NPD at 10 K; a = 7.2599(5) Å, c = 11.716(1) Å; R_{wp} = 0.0222, R_p = 0.0183, and χ^2 = 1.139						
Ba	2*b*	1.0	2/3	1/3	0.228(3)	0.08(1)
B1	6*c*	1.0	0.925(2)	0.394(2)	0.893(2)	0.0182(4)
B2	6*c*	1.0	0.510(2)	0.297(2)	0.981(1)	0.0182(4)
B3	6*c*	1.0	0.826(2)	0.368(2)	0.748(1)	0.0182(4)
B4	6*c*	1.0	0.417(1)	0.289(2)	0.834(2)	0.0182(4)
H1	6*c*	1.0	0.102(2)	0.445(2)	0.905(2)	0.044(2)
H2	6*c*	1.0	0.404(3)	0.263(3)	0.059(1)	0.044(2)
H3	6*c*	1.0	0.918(3)	0.374(4)	0.667(2)	0.044(2)
H4	6*c*	1.0	0.252(2)	0.265(3)	0.811(2)	0.044(2)

of the B–B distances is caused in part by the slight displacements (from the ideal icosahedral positions) of the apical B atoms (*i.e.*, B1 and B4) of the pentagonal pyramids on the sides of the $B_{12}H_{12}^{2-}$ anions. Such displacements are undoubtedly affected by the unequal/asymmetric attractive interactions from the adjacent Ba^{2+} cations and the repulsive interactions from the surrounding $B_{12}H_{12}^{2-}$ anions. Moreover, for the B atoms comprising the top (*i.e.*, B3) and bottom (*i.e.*, B2) triangles of the $B_{12}H_{12}^{2-}$ anions (*i.e.*, parallel to the *ab*-basal plane), the interactions from the surrounding $B_{12}H_{12}^{2-}$ and Ba^{2+} ions are symmetric. Thus these triangles are equilateral, *i.e.*, each display equal B–B distances (although these distances differ for the top and bottom triangles). In general, the overall distortion of the $B_{12}H_{12}^{2-}$ anions is a result of their actual orientation with respect to the surrounding cations and anions in the crystal structure.

DFT calculations confirmed the stability of the *P*31*c* structure (see Table S4 in the SI for the DFT-optimized coordinates). The neutron vibrational spectra at 4 K for $SrB_{12}H_{12}$ and $BaB_{12}H_{12}$ were found to be in excellent agreement with the calculated phonon densities of states based on the DFT-optimized *P*31*c* structures (see SI Fig. S2 [17]). Previous reports [2–4,17] have indicated that the phonon density of states is sensitive to the structural details of the $B_{12}H_{12}^{2-}$ lattice arrangements and can be used to verify particular structural models. With respect to structural stability at higher temperatures, the TGA-DSC measurements of both compounds showed no evidence of a structural phase change between 295 and 950 K.

The *P*31*c* structural arrangements for $SrB_{12}H_{12}$ and $BaB_{12}H_{12}$ differ somewhat from those observed when the Ae^{2+} cation is even smaller, as in $CaB_{12}H_{12}$ (with a Ca^{2+} Pauling radius of 0.99 Å) [16], where each anion and cation is now located near the base (in three-fold coordination) rather than at the center (in four-fold coordination) of its counter-ion tetrahedron [4]. Indeed, similar behavior is observed in the $A_2B_{12}H_{12}$ compounds [3], where

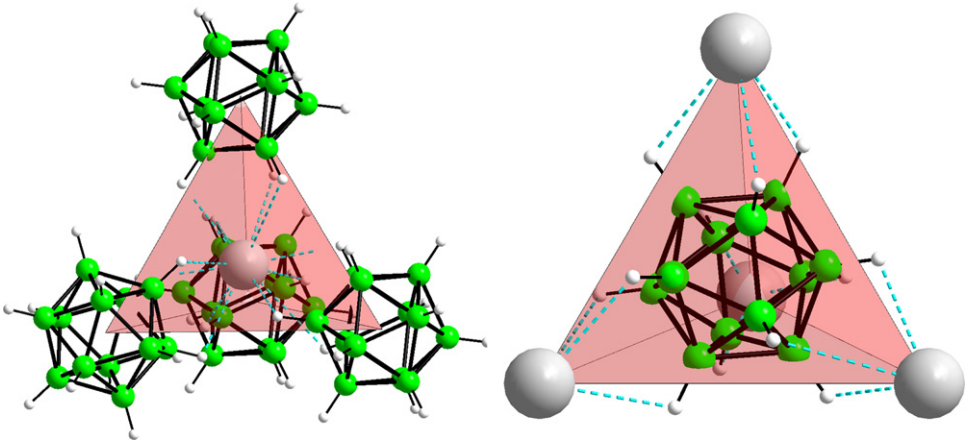

Fig. 3. The surroundings of the Sr^{2+} or Ba^{2+} cations (left) and the $B_{12}H_{12}^{2-}$ anion (right) of the *P*31*c*-symmetric structure.

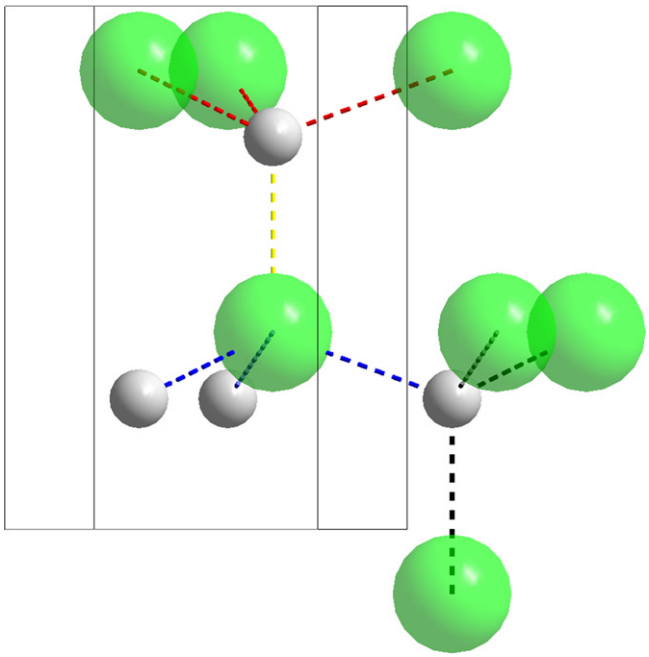

Fig. 4. Packing diagram showing the $B_{12}H_{12}^{2-}$ anions (large green spheres) and Sr^{2+} or Ba^{2+} cations (small gray spheres). (For interpretation of the references to color in this figure legend, the reader is referred to the web version of the article.)

decreasing the size of the A^+ cation from K^+ to Li^+ (with Pauling radii of 1.33 and 0.60 Å, respectively) [16] also leads to a shift in the location of the cation from the center towards the base of the $B_{12}H_{12}^{2-}$ anion tetrahedron.

It is interesting to analyze the variation in $AeB_{12}H_{12}$ structural arrangements based on simple geometric packing criteria [18–21]. Accordingly, planar three-fold coordination is favored when the cation–anion radius ratio r_c/r_a is between 0.155 and 0.225. Tetrahedral four-fold coordination is favored for larger ratios between 0.225 and 0.414. Two-fold coordination is favored for ratios below 0.155. To determine these ratios for the $AeB_{12}H_{12}$ compounds, one must estimate an effective radius r_a in these structures for the quasi-spherical $B_{12}H_{12}^{2-}$ anion. From the current results at 295 K, the average nearest-neighbor distances d_{a-c} between the centers of the anions and cations are ≈4.30 and 4.47 Å for $SrB_{12}H_{12}$ and $BaB_{12}H_{12}$, respectively. Moreover, for Sr^{2+} and Ba^{2+} cations in four-fold coordination, a reasonable extrapolation from alkaline-earth cation radii data for higher coordination numbers as tabulated and plotted by Shannon [22] yields effective cation radii r_c of ≈1.03 and 1.20 Å, respectively, smaller than their Pauling radii values. Assuming $d_{a-c} = r_a + r_c$ results in an r_a value of ≈3.27 Å for both $SrB_{12}H_{12}$ and $BaB_{12}H_{12}$. This yields respective r_c/r_a ratios of 0.31 and 0.37 for the former and latter, which are within the 0.225–0.414 range favoring tetrahedral four-fold coordination, as observed.

In the case of $CaB_{12}H_{12}$, it seems that a smaller cation radius than those of Sr^{2+} and Ba^{2+} allows the $B_{12}H_{12}^{2-}$ anions to approach each other too closely in tetrahedral coordination, causing an additional increase in anion–anion repulsion, thus lowering the overall cohesive energy of the crystal lattice [3]. From the $CaB_{12}H_{12}$ structure at 293 K [4], the average nearest-neighbor anion–cation distance d_{a-c} is ≈4.09 Å. For the three-fold coordinated Ca^{2+} cation, again an extrapolation from Ca^{2+} cation radii data for higher coordination numbers from Shannon [22] yields an r_c of ≈0.75 Å. This results in r_a and r_c/r_a values of 3.34 Å and 0.22, respectively. The latter value, in contrast to the larger r_c/r_a values for $SrB_{12}H_{12}$ and $BaB_{12}H_{12}$, is just within the 0.155–0.225 range favoring three-fold coordination, again as observed. Thus, in the case of $CaB_{12}H_{12}$, the *P*31*c* structure of $SrB_{12}H_{12}$ and $BaB_{12}H_{12}$ with its tetrahedral coordination is no longer the most stable configuration, and a combination of lattice distortions, cation displacements, and correlated $B_{12}H_{12}^{2-}$ anion reorientations resulting in three-fold coordinations is needed to maximize the cohesive energy. Hence, the observed structure for the lighter $CaB_{12}H_{12}$ is not trigonal (*P*31*c*), but monoclinic (*C*2/*c*).

It would be interesting to see what type of structure is favored for the dodecahydro-*closo*-dodecaborate of the even lighter and smaller Mg^{2+} cation, $MgB_{12}H_{12}$, but this awaits some breakthrough in the procedures to synthesize such a compound. Work is currently progressing along this direction. Nonetheless, first-principles calculations [5] have suggested that, because of the even smaller Mg^{2+} cation, the most stable $MgB_{12}H_{12}$ structure should entail Mg^{2+} two-fold coordination to the $B_{12}H_{12}^{2-}$ anions, and not three-fold coordination. Again an extrapolation from Mg^{2+} cation radii data for higher coordination numbers from Shannon [22] yields r_c values of ≈0.48 and 0.38 Å for three-fold and two-fold-coordinated Mg^{2+}, respectively. Hence, the respective low r_c/r_a ratios of 0.14 and 0.11, indeed favor two-fold coordination, based on geometric packing criteria.

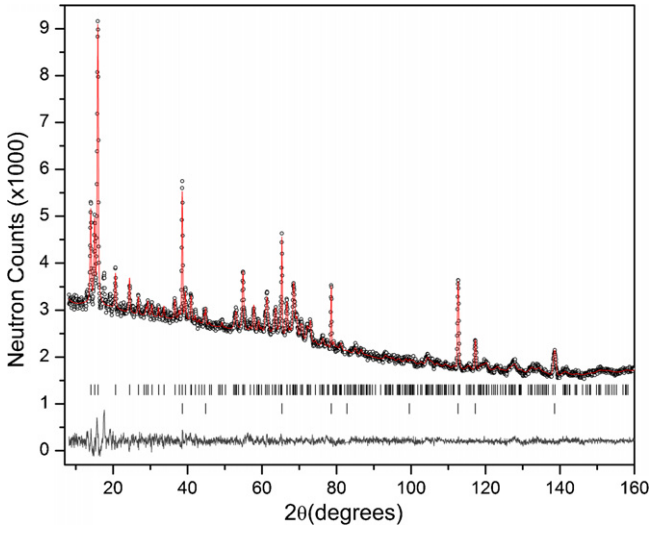

Fig. 5. Experimental (circles), calculated (line), and difference (line below observed and calculated patterns) NPD profiles for $Ba(^{11}B)_{12}H_{12}$ at 10 K. The pattern also contains peaks from a $Ba(H_2O)_6(^{11}B)_{12}H_{12}$ impurity [8] at ≈17.5° and 19.5°, and from Al foil wrap. The upper and lower sets of vertical bars indicate the calculated positions of Bragg peaks for $Ba(^{11}B)_{12}H_{12}$ and Al, respectively.

4. Conclusions

Both $SrB_{12}H_{12}$ and $BaB_{12}H_{12}$ were found to possess the same novel *P*31*c*-symmetric trigonal structure with tetrahedral four-fold ion coordinations. This structure appears to be stable for both compounds up to at least 950 K, and represents the preferred arrangement of alkaline-earth cations and $B_{12}H_{12}^{2-}$ anions for Ae^{2+} cations above a certain size. This is not the structure found for the smaller-cation analog, $CaB_{12}H_{12}$, where an alternative monoclinic arrangement of the anions and cations with three-fold coordinations is necessary to maximize the cohesive energy.

Acknowledgements

This work was partially supported by DOE through EERE Grant Nos. DE-AI-01-05EE11104, DE-EE0002978, and DE-AC04-94AL85000.

Appendix A. Supplementary data

Supplementary data associated with this article can be found, in the online version, at doi:10.1016/j.jallcom.2011.10.085.

References

[1] S.-J. Hwang, R.C. Bowman Jr., J.W. Reiter, J. Rijssenbeek, G.L. Soloveichik, J.-C. Zhao, H. Kabbour, C.C. Ahn, J. Phys. Chem. C 112 (2008) 3164.
[2] J.-H. Her, M. Yousufuddin, W. Zhou, S.S. Jalisatgi, J.G. Kulleck, J.A. Zan, S.-J. Hwang, R.C. Bowman Jr., T.J. Udovic, Inorg. Chem. 47 (2008) 9757.
[3] J.-H. Her, W. Zhou, V. Stavila, C.M. Brown, T.J. Udovic, J. Phys. Chem. C 113 (2009) 11187.
[4] V. Stavila, J.-H. Her, W. Zhou, S.-J. Hwang, C. Kim, L.A.M. Ottley, T.J. Udovic, J. Solid State Chem. 183 (2010) 1133.
[5] V. Ozolins, E.H. Majzoub, C. Wolverton, J. Am. Ceram. Soc. 131 (2009) 230.
[6] X. Chen, H.K. Lingam, Z. Huang, T. Yisgedu, J.-C. Zhao, S.G. Shore, J. Phys. Chem. Lett. 1 (2010) 201.
[7] Certain commercial suppliers are identified in this paper to foster understanding. Such identification does not imply recommendation or endorsement by the NIST nor does it imply that the materials or equipment identified are necessarily the best available for the purpose.
[8] I. Tiritiris, T. Schleid, Z. Anorg. Allg. Chem. 627 (2001) 1836.
[9] J.K. Stalick, E. Prince, A. Santoro, I.G. Schroder, J.J. Rush, in: Neutron Scattering in Materials Science, edited by D.A. Neumann, T.P. Russell, B.J. Wuensch, Vol. II. Mater. Res. Soc. Symp. Proc. No. 376, Materials Research Society, Pittsburgh, PA, 1995, p. 101.
[10] A.C. Larson, R.B. Von Dreele, General Structure Analysis System (GSAS), Los Alamos National Laboratory Report LAUR 86-748, 2000.
[11] B.H. Toby, J. Appl. Crystallogr. 34 (2001) 210.
[12] T.J. Udovic, C.M. Brown, J.B. Leão, P.C. Brand, R.D. Jiggetts, R. Zeitoun, T.A. Pierce, I. Peral, J.R.D. Copley, Q. Huang, D.A. Neumann, R.J. Fields, Nucl. Instrum. Methods A 588 (2008) 406.
[13] Quantum-ESPRESSO package: www.pwscf.org.
[14] G. Kresse, J. Furthmuller, J. Hafner, Europhys. Lett. 32 (1995) 729.
[15] T. Yildirim, Chem. Phys. 261 (2000) 205.
[16] J.E. Huheey, E.A. Keiter, R.L. Keiter, Inorganic Chemistry: Principles of Structure and Reactivity, 4th ed., HarperCollins, New York, 1993.
[17] N. Verdal, W. Zhou, V. Stavila, J.-H. Her, M. Yousufuddin, T. Yildirim, T.J. Udovic, J. Alloys Compd. 509S (2011) S694.
[18] G.F. Hüttig, Z. Anorg. Chem. 113 (1920) 24.
[19] V. Goldschmidt, Trans. Faraday Soc. 25 (1929) 253.
[20] L. Pauling, J. Am. Ceram. Soc. 51 (1929) 1010.
[21] L.C. Nathan, J. Chem. Educ. 62 (1985) 215.
[22] R.D. Shannon, Acta Crystallogr. A 32 (1976) 751.